AIDA

Advanced European Infrastructures for Detectors at Accelerators

Scientific / Technical Note

Parametrisation of hadron shower profiles in the CALICE Sc-Fe AHCAL

Chadeeva, M (ITEP)

03 April 2014

The research leading to these results has received funding from the European Commission under the FP7 Research Infrastructures project AIDA, grant agreement no. 262025.

This work is part of AIDA Work Package **9: Advanced infrastructures for detector R&D**.

CALICE Analysis Note CAN-048
April 3, 2014

Parametrisation of hadron shower profiles in the CALICE Sc-Fe AHCAL

The CALICE Collaboration [1]

Abstract

The spatial shower development in the CALICE scintillator-steel analogue hadronic calorimeter was studied using test beam data collected at CERN and FNAL for single positive hadrons with initial momenta from 10 to 80 GeV/c. The parametrisation of both longitudinal and radial profiles are fit to test beam data and simulations using physics lists from GEANT4 version 9.6. The parameters extracted from data and simulated samples are compared for different types of hadrons.

[1]Corresponding author: Marina Chadeeva; marina@itep.ru

Contents

1 Introduction **2**

2 Data, software and event selection **3**

3 Systematic uncertainties **4**

3.1 Layer-to-layer variations 5

3.2 Identification of the shower start layer 6

3.3 Reconstruction of the shower axis 7

3.4 Pion contamination of the proton samples 8

3.5 Positron contamination in the samples taken without ECAL 9

3.6 Longitudinal leakage from the AHCAL 10

4 Ratio of hadron shower profiles **10**

4.1 Ratio of longitudinal profiles 10

4.2 Ratio of radial profiles 11

5 Parametrisation and fit of hadron shower profiles **12**

5.1 Fit to longitudinal profiles 12

5.2 Fit to radial profiles 14

6 Comparison of shower profile parameters **18**

6.1 Tail and halo parameters 18

6.2 "Short" and core parameters 18

7 Conclusion **19**

1 Introduction

The development of a hadronic shower in a calorimeter is a complicated process that is characterised by significant fluctuations of the measured energy as well as the measured longitudinal and radial shower sizes. The understanding of hadronic showers and their parametrisation is important for the estimation of leakage from the calorimeter, for the validation of hadronic shower models in simulations and for the development of particle flow algorithms.

Hadronic showers induced by mesons and baryons are observed to give different response in the calorimeter. This can be mainly explained by the baryon number conservation law and therefore different available energy. The latest study of such a comparison performed with the scintillator-iron ATLAS Tile calorimeter can be found in [1]. The comparison of different types of hadrons described in the previous studies was hampered by the difference in nuclear interaction lengths — the analysis was performed of the energy density distributions convoluted with the distribution of the shower start position. The high granularity of the CALICE AHCAL gives a possibility to identify the position of the first inelastic interaction and hence to disentangle the spatial shower development from the distribution of the shower start position.

The behaviour of hadronic showers can be described by so called global observables, such as the deposited energy, shower radius, and longitudinal centre of gravity. The detailed study of these observables including the comparison between data and simulations using the GEANT4 package [2] is presented in [3]. For all studied energies, proton showers were found to be on average ∼5% longer and ∼10% wider than pion showers. The GEANT4 physics lists used in the comparison give better predictions for protons than for pions and predict a steeper energy dependence of the calorimeter response than observed in data. The prediction of the mean shower radius was significantly improved in the version GEANT4 9.6, where the agreement with data is now within 5% in the entire energy range studied.

It is obvious that global observables might shadow or smear detailed differences. The high longitudinal and transverse granularity of the CALICE AHCAL allows to perform more detailed comparisons of the shower development in data and simulations using shower profiles. A typical shower induced by different types of hadrons consists of a relatively narrow core with high energy density surrounded by an extended halo. The core is interpreted as being formed by electromagnetic cascades arising from the decays of π^0 mesons produced in hard interactions in the shower start phase. In this note, longitudinal and transverse shower profiles are decomposed into core and halo contributions by fitting an empirical parametrisation to the energy density distributions extracted from both data and simulations. The fitted parameters and the extracted core shower fractions are compared to simulations using recent GEANT4 physics lists.

The second section presents the experimental setup and the event selection procedure. The third section is dedicated to the estimation of systematic uncertainties. The ratios of longitudinal and radial profiles are shown in the fourth section. The parametrisation of

Table 1: List of positive hadron data runs used in the analysis and sample statistics.

Run number	Beam momentum GeV/c	Total number of events	Fraction of μ^+	Fraction of e^+	Fraction of multi-particle	Number of selected π^+	Number of selected protons
580060	10	45839	3.0%	37.2%	13.2%	5275	1239
580063	15	46323	3.8%	19.9%	13.7%	6660	2122
331340	30	192066	30.1%	n/e*	0.2%	10836	7713
331339	40	201019	4.6%	n/e	0.3%	20931	4798
331337	50	199829	4.4%	n/e	0.3%	21150	4190
331334	60	208997	3.8%	n/e	0.3%	21131	5756
331324	80	197062	2.8%	n/e	0.3%	16963	8541

* n/e - not estimated because of the requirement of a track in the electromagnetic calorimeter for selected hadron events.

profiles is discussed in the fifth section. The sixth section contains a comparison of profile parameters extracted from data and simulated samples for both pion and proton-induced showers.

2 Data, software and event selection

The analysis is based on positive hadron data collected during CALICE test beams at CERN in 2007 and at FNAL in 2009. The CALICE setup at CERN is described in detail in [4] and comprised the Si-W electromagnetic calorimeter (ECAL) [5], the Sc-Fe AHCAL [6] and the Sc-Fe tail catcher and muon tracker (TCMT) [7]. Positive pion beams in the momentum range from 30 to 80 GeV/c were delivered from the CERN SPS H6 beam line. The data from a threshold Čerenkov counter upstream of the calorimeter setup was used for off-line discrimination between pions and protons on an event-by-event basis.

The CALICE setup during the test beam campaign at FNAL is described in detail in [9]. In the current analysis, test beam data collected at FNAL without electromagnetic calorimeter at initial momenta of 10 and 15 GeV/c were considered. The off-line event-by-event separation of pions and protons was performed using both signals of the differential Čerenkov counter placed upstream of the calorimeter setup.

The list of runs used for the current analysis is presented in Table 1. All runs were taken at normal incidence of beam particles w.r.t. the calorimeter front plane. The sizes of π^+ and protons samples selected for the current analysis as described below are listed in the last two columns of Table 1.

The energy reconstruction was performed using CALICE software version v04-07. The visible signal in each calorimeter cell is obtained in units of MIP (minimum-ionising

particle) as described in [6]. Only cells with a signal above 0.5 MIP were considered for further analysis and are called hits. The hadron event selection procedure comprises several steps and involves also the procedures of shower start and primary track finding. A detailed description of the event selection procedure can be found in [3] including the estimates for the purity of the proton samples. The shower start finding algorithm is described in detail in [10] and estimations of its quality using simulated samples are given in [11].

The simulations were done using the software packages Mokka v08_02 [8] and GEANT4 version 9.6 patch 1, accompanied by the digitisation procedure from calice_soft v04-07 (with the conversion coefficient 846 keV/MIP and light crosstalk 0.15 for the AHCAL). The profile of the test beam and its position on the calorimeter front face in each data run were closely reproduced in simulations. Two physics lists were studied: QGSP_BERT and FTFP_BERT. The detailed description of the involved models can be found in [2, 9].

Events, well contained in the AHCAL, were selected from both data and simulated samples for further analysis of shower profiles. For runs taken without ECAL, we selected events with an identified shower start in physical layers 3, 4, 5, 6, to minimise leakage and reduce the fraction of remaining positrons in the sample. The events with identified shower start in physical layers 2, 3, 4, 5, 6 were used for runs taken with the ECAL in front to minimise the leakage into the TCMT. The first physical layer was excluded due to uncertainties of the shower start identification. Hereinafter the profiles from the identified shower start are analysed.

The longitudinal depth is measured in units of effective nuclear interaction length $\lambda_{\mathrm{I}}^{\mathrm{eff}}$ which is estimated to be 231 mm for the Sc-Fe AHCAL. The total depth of the Sc-Fe AHCAL is $\sim 5.3\lambda_{\mathrm{I}}^{\mathrm{eff}}$ (38 physical layers with $\sim 0.137\lambda_{\mathrm{I}}^{\mathrm{eff}}$ per layer). The first section of TCMT consists of 9 physical layers comprised of 2-cm thick steel absorber plates and 5-mm thick scintillator strips and has the same sampling as the AHCAL ($\sim 0.14\lambda_{\mathrm{I}}^{\mathrm{eff}}$ per layer). Although the data from the TCMT is not used for fits to avoid problems with intercalibration, the longitudinal shower development (except for profile ratios) is shown in both AHCAL and the first part of the TCMT up to $\sim 6.5\lambda_{\mathrm{I}}^{\mathrm{eff}}$ (47 physical layers in total). The units of effective radiation length $X_0^{\mathrm{eff}} = 25.5$ mm are also used, where appropriate.

In contrast to longitudinal profiles, transverse profiles cannot be calculated in the TCMT because the latter is assembled from strips which do not allow simultaneous determination of both transverse coordinates. The radial distances are measured in mm. It should be mentioned that the effective Molière radius for the Sc-Fe AHCAL, $R_{\mathrm{M}}^{\mathrm{eff}}$, equals to 24.5 mm.

3 Systematic uncertainties

There are several sources of systematic uncertainties which can affect the shape of the shower profiles studied in this note:

- layer-to-layer variations of the response;

- identification of the shower start layer;
- identification of the shower axis for radial profiles;
- pion contamination of the proton samples;
- positron contamination of samples collected without electromagnetic calorimeter;
- leakage from the AHCAL.

3.1 Layer-to-layer variations

Imperfections in the calibration procedure, temperature correction and saturation estimation as well as several percent of dead and noisy cells lead to variations of the measured response. As a result the longitudinal profile, plotted from the calorimeter front, is non-smooth [12]. The most significant contribution to these variations come from the saturation correction procedure, which involves uncertainties in the SiPM response function. This statement is supported by the fact that variations increase with beam energy, the largest variations are observed at 80 GeV. The variations also depend on the conditions in a particular run, e.g. the temperature and beam profile that determines which calorimeter cells are hit. The analysis of profiles from shower start helps to minimise layer-to-layer variations due to the averaged contributions from different physical layers. Nevertheless, these profiles still remain non-smooth when a narrow range of starting layers is used in the event selection (e.g. four or five in the current analysis), as shown in Fig. 1a.

Fig. 1 shows separate longitudinal profiles for events with shower start in a particular physical layer of the AHCAL, as well as the mean of these profiles. All profiles are normalised by the number of events. In case of an ideal calorimeter, these shower profiles should not depend on the shower start position (except for several last layers as the profiles with later start are shorter). Therefore, the difference between profiles with different shower start positions can be interpreted as systematic uncertainty. To quantify the systematic uncertainty, the following procedure is used. The single profiles for different fixed shower start layers are considered to be a sample of size n, where n is the number of separate profiles (e.g. n =3 in Fig. 1). Each profile has m bins. The content of i-th bin of j-th profile is e_{ij}, where $1 < i < m$ and $1 < j < n$. The bin content of the mean profile, averaged over the single profiles, is $E_i = \sum_{j=1}^{n} e_{ij}/n$. The variance of the bin content for the sample of profiles is $s_i = \sum_{j=1}^{n} (e_{ij} - E_i)^2/(n-1)$. The mean of profiles is assumed to be an estimate of the true profile and is used for the analysis. The corresponding uncertainty in the i-th bin due to variations between the single profiles is calculated as $\sqrt{s_i/n}$ and is shown with the yellow band in Fig. 1.

The same procedure is applied to the simulated samples for which the variations are observed to be smaller than for the data, as shown in Fig. 1b. These layer-to-layer variations in the simulated samples appear due to taking into account the list of dead cells and cell-wise noise addition in the digitisation procedure. At the same time, the

main source of variations observed in the real calorimeter arises from imperfections in the saturation correction, which are not simulated.

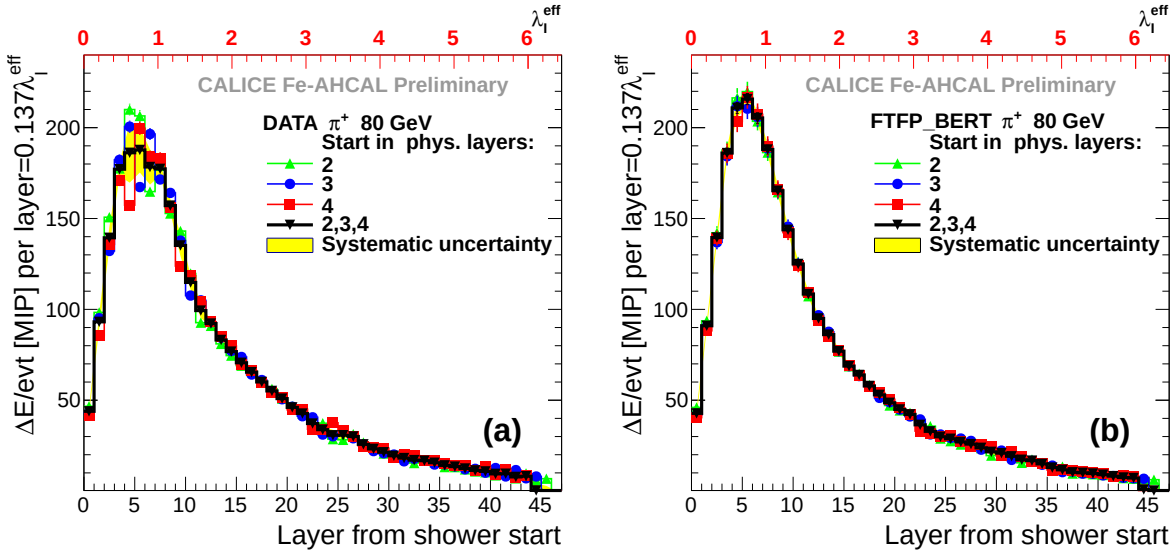

Figure 1: Longitudinal profiles of showers induced by pions with an initial energy of 80 GeV in the AHCAL obtained (a) from data and (b) simulated samples. The profiles for events with identified shower start in physical layer 2 (red circles), physical layer 3 (blue squares) or physical layer 4 (green triangles) are plotted separately. The black histogram is a mean of the three coloured histograms. The yellow band corresponds to the systematic uncertainty (see section 3.1 for details).

The same approach is applied to estimate the systematic uncertainties for radial profiles. Although the impact of layer-to-layer variations on radial profiles is smaller as they are integrated along the longitudinal coordinate, there is another source of systematic uncertainty that is related to the determination of the shower axis and will be discussed below in section 3.3.

3.2 Identification of the shower start layer

The same procedure of shower start layer identification is applied to all samples, therefore possible uncertainties of the procedure are included in the distributions obtained from both data and simulated showers. At the same time, the uncertainty of the algorithm can affect the comparison of shower profiles at different energies (i.e. distort the energy dependence of shower profile parameters) for the following reasons: (a) the accuracy of the algorithm degrades with decreasing energy and (b) its uncertainty is larger for the very first physical layers of the calorimeter setup[2]. Therefore one can expect a bigger

[2]The algorithm includes a calculation of moving average of the energy deposition per layer within a window of 10 layers. For the first nine physical layers it is assumed that the deposition before the first layer corresponds to incoming track and equals to 1.3 MIP. The procedure is described in detail in [10].

uncertainty due to shower start finder algorithm for samples below 20 GeV taken at FNAL with the setup configuration without the ECAL. To understand the impact of the shower start finder algorithm, the simulated samples of negative pions for two setup configurations were compared as shown in Fig. 2, where the profiles are plotted for selected events with a found shower start behind the second physical layer of the AHCAL. The differences between the shown profiles are within the uncertainties estimated in section 3.1 and will not be introduced as additional systematic uncertainties in the following analysis. It should be noted that simulated profiles for positive and negative pions also coincide within statistical uncertainties.

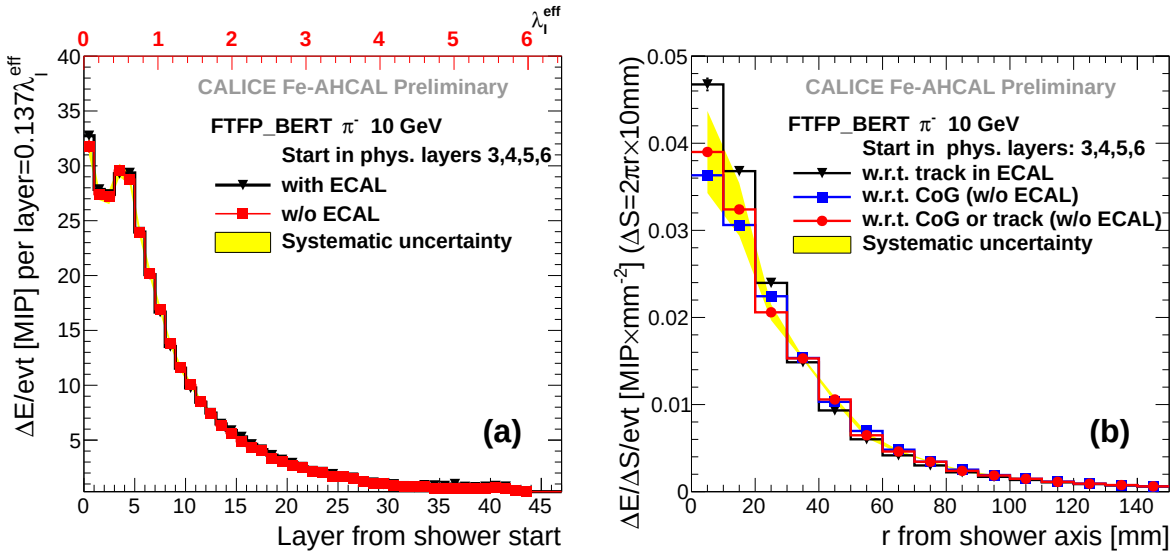

Figure 2: Shower profiles of simulated negative pions with initial energy 10 GeV which start showering in physical layers 3,4,5 or 6 of the AHCAL: (a) longitudinal profiles obtained with (black triangles) and without (red circles) ECAL, (b) radial profiles w.r.t. shower axis estimated from track in ECAL (black triangles), shower centre of gravity (blue squares) and combined method (red circles). The yellow band shows the systematic uncertainty (see sections 3.1 and 3.3 for details).

3.3 Reconstruction of the shower axis

A reference axis for calculating the radial shower profile is defined by the incoming track which coordinates are reconstructed on an event-by-event basis. The primary track coordinates in the setup configuration with the ECAL are calculated from identified track hits with relatively good precision due to high granularity of the ECAL (1×1 cm^2 cells). This is not possible in the configuration without the ECAL, but two alternative approaches are available: estimation of the event centre of gravity or identification of the incoming track in the AHCAL. A reliable track identification requires at least four points, hence it is not applicable to showers that start before the fifth physical layer of the AHCAL. Moreover, the AHCAL central cell transverse size is three times larger than that of the

ECAL cell which leads to a lower accuracy of the primary track position (shower axis) extracted from track hits in the AHCAL. The event centre of gravity is identified with high precision due to the large number of hits (100 and more) but might be shifted w.r.t. primary track due to the asymmetry of shower or instrumental effects (e.g. dead or noisy cells).

Figure 2b shows the radial profiles of simulated pion showers obtained using different methods of shower axis identification. The reconstruction of the shower axis from tracks in the ECAL results in a higher energy density in the core region while the application of the centre of gravity underestimates the contribution near the shower axis. The red circles correspond to the combined method used in the current analysis where the shower axis is extracted from the centre of gravity for events with the shower start in physical layers 3 and 4 and from the track hits in the AHCAL for events with the start in physical layers 5 and 6. The systematic uncertainty shown with the yellow band in Fig. 2b also includes the uncertainty due to differences between the two methods of shower axis reconstruction. As follows from Fig. 2b the most significant contribution of these uncertainties is in the region near the shower axis where they amount up to 10%.

3.4 Pion contamination of the proton samples

The inefficiency of the Čerenkov counter leads to a contamination of the proton samples in the test beam data. The estimation of the Čerenkov counter efficiency is based on an independent procedure of identifying muons in the same run. The efficiency estimates are then used to calculate the purity of the proton samples η, as described in [3]. The values of η in the current analysis vary from 74% to 95%. For global observables, the impurity was propagated to the systematic uncertainty of the corresponding estimates for protons, as also described in [3]. Another approach is used to extract parameters from the fit to the shower profiles. We assume that the analysed pion samples are not contaminated and correct the proton profiles taking into account the proton sample purity η estimated for the given run. The content of each bin of the proton profile is corrected by subtracting the estimated contribution obtained from the pure pion profile in the following way:

$$\Delta E_i^{\mathrm{corr}} = \Delta E_i^{\mathrm{mix}} \cdot \frac{1}{\eta} - \Delta E_i^{\pi} \cdot \frac{1-\eta}{\eta}, \tag{1}$$

where $\Delta E_i^{\mathrm{corr}}$ is the corrected content of i-th bin of the proton profile, $\Delta E_i^{\mathrm{mix}}$ is the content of i-th bin in the profile for the mixed sample and ΔE_i^{π} is the content of i-th bin in the profile obtained for pions of the same energy. The same correction procedure was applied to longitudinal and radial profiles of proton-induced showers in test beam data. The resulting uncertainty of the corrected energy deposition in the particular bin is calculated using standard error propagation techniques taking into account the estimated statistical and systematic uncertainties of all variables involved: $\Delta E_i^{\mathrm{mix}}$, ΔE_i^{π} and η.

3.5 Positron contamination in the samples taken without ECAL

The positron contamination of hadron samples in the runs taken without ECAL can be significantly reduced by the selection procedure described in [3]. The additional selection of events with shower start behind the second AHCAL layer helps to remove remaining positrons. As there were no positive hadron runs below 30 GeV taken with the ECAL being in front of the AHCAL, we use negative pion runs at 10 and 15 GeV to perform a crosscheck.

Fig. 3 shows the longitudinal profiles from shower start for pions with an initial energy of 15 GeV for data taken with different setup configurations: with the ECAL in front of the AHCAL for negative pions and without the ECAL for positive pions. Due to the ECAL the negative pion samples are assumed to have no electron contamination. The differences between profiles of the negative and positive pions shown in Fig. 3a for selected events with the shower start in physical layers 3,4,5,6 of the AHCAL are within the uncertainties estimated in section 3.1. On the other hand, the difference due to positron admixture in data taken without the ECAL is shown for comparison in Fig. 3b where profiles plotted for selected events with the shower start in physical layers 1,2 are shown. Therefore, one can conclude that the positron contamination does not affect shower profiles for selected events with the shower start positions behind the second physical layer of the AHCAL and hence will not be introduced as additional systematic uncertainty.

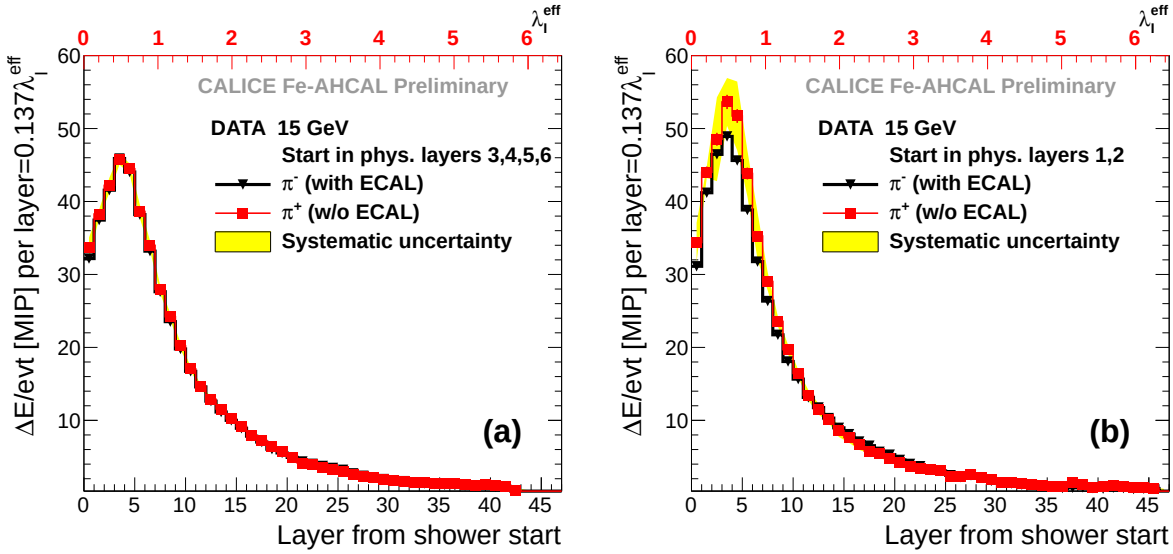

Figure 3: Longitudinal profiles of showers induced by negative pions from test beam data (setup with ECAL, black triangles) and positive pions (setup w/o ECAL, red circles) with initial energy 15 GeV for selected events with the identified shower start in physical layers (a) 3,4,5,6 and (b) 1,2 of the AHCAL. The yellow band corresponds to the systematic uncertainty (see section 3.1 for details).

3.6 Longitudinal leakage from the AHCAL

The selection of the shower start at the beginning of the AHCAL helps to minimise longitudinal leakage. Nevertheless, the AHCAL depth of $\sim 5.3\lambda_{\mathrm{I}}^{\mathrm{eff}}$ is not enough to contain the entire hadronic shower, even if it is induced by a particle with initial energy 30 GeV. The restriction of the range used to fit the shower profile can affect the estimation of parameters. The uncertainty due to the cut on the fit range of the longitudinal profiles was estimated by the following procedure. The histogram was generated from an analytical function used for the profile parametrisation (see section 5.1) with the parameters obtained from the fit to data or simulations. The bin contents were then smeared within real uncertainties, these uncertainties being assigned to bin errors. Then the generated histogram was fit with different upper limits of the fit range (from $4\lambda_{\mathrm{I}}^{\mathrm{eff}}$ to $7\lambda_{\mathrm{I}}^{\mathrm{eff}}$) and the fit results were compared. The differences in the obtained parameters were found to be more than 3 times smaller than the uncertainties of the fit.

4 Ratio of hadron shower profiles

The current analysis is dedicated to the study of shower profiles from the identified shower start position. The quality of Monte Carlo predictions of shower development can be illustrated using the ratios of shower profiles extracted from simulated events to those extracted from test beam data. Such a comparison with the physics lists from GEANT4 version 9.4 was done in [12]. It should be noted that in the current note the comparison is performed with GEANT4 version 9.6, and the event selection and profile normalisation procedures differ from those used in [12], so the analyses cannot be directly compared.

4.1 Ratio of longitudinal profiles

The longitudinal profiles from shower start represent the visible energy in units of MIP measured per calorimeter layer, where the first bin corresponds to the physical layer where the shower start is identified. Fig. 4, 5 and 6 show the ratios of longitudinal profiles obtained from simulated samples (by FTFP_BERT or QGSP_BERT physics list) to those extracted from test beam data.

The proton profiles are well reproduced by the FTFP_BERT physics list at all studied energies. For energies below 20 GeV, the profiles of pion showers are reproduced by FTFP_BERT within 5%. The overestimation of deposition around the shower maximum increases with energy up to $\sim$12% at 80 GeV. The tail of the shower is well reproduced at all energies.

The QGSP_BERT physics list underestimates energy deposition for pions at 10 GeV, gives a good prediction at 15 GeV and significantly overestimates the amount of energy deposited around the shower maximum for both pions and protons at higher energies,

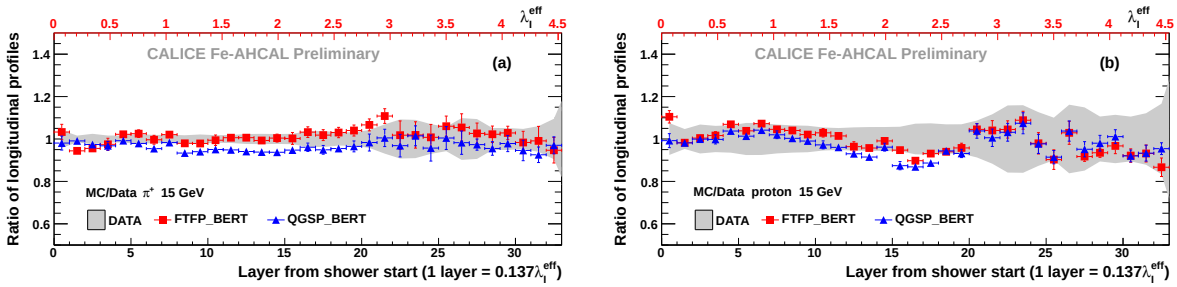

Figure 4: Ratio of longitudinal profiles of showers induced by 15 GeV hadrons from simulated samples to those from data samples for (a) pions and (b) protons. The grey band and the error bars show the uncertainty for data and simulations, respectively.

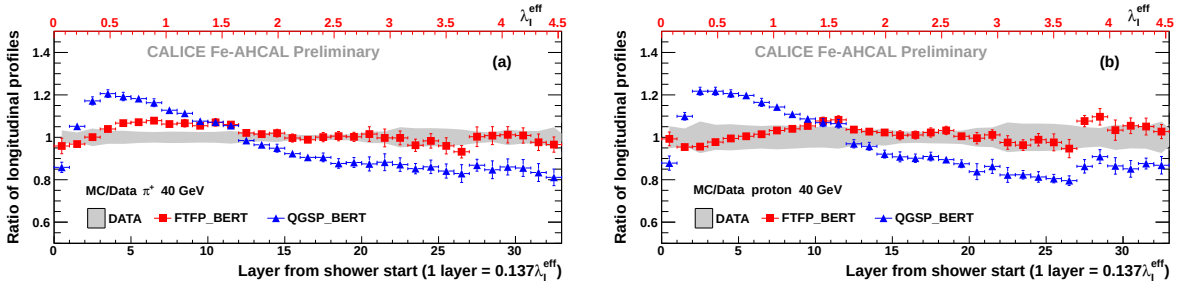

Figure 5: Ratio of longitudinal profiles of showers induced by 40 GeV hadrons from simulated samples to those from data samples for (a) pions and (b) protons. The grey band and the error bars show the uncertainty for data and simulations, respectively.

showing more than 20% excess at 80 GeV. The deposition in the tail of the shower is underestimated by this physics list.

4.2 Ratio of radial profiles

The radial shower profile is the distribution of the energy density, measured in the ring of radius r and width Δr, with the distance r to the shower axis (for this analysis we use $\Delta r = 10$ mm), integration along longitudinal direction being assumed. The shower axis in turn can be extracted either from track coordinates (if a track in ECAL can be reconstructed) or from the event's centre of gravity. The hits in physical layers before the shower start layer are not included in the radial profiles. Fig. 7, 8 and 9 show the ratios of radial profiles obtained from simulated samples (by FTFP_BERT or QGSP_BERT physics list) to those extracted from test beam data.

The comparison of radial profiles demonstrates a similar tendency as observed for longitudinal ones. The radial development of proton showers is predicted by the FTFP_BERT physics list within systematic uncertainties. The deposition near the shower axis is overestimated by FTFP_BERT for pions by up to 20% at 80 GeV and significantly overestimated by QGSP_BERT for both pions and protons (up to 30%).

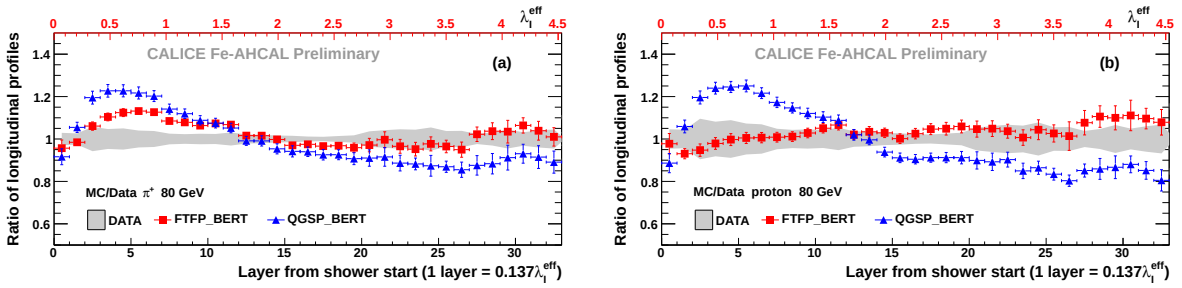

Figure 6: Ratio of longitudinal profiles of showers induced by 80 GeV hadrons from simulated samples to those from data samples for (a) pions and (b) protons. The grey band and the error bars show the uncertainty for data and simulations, respectively.

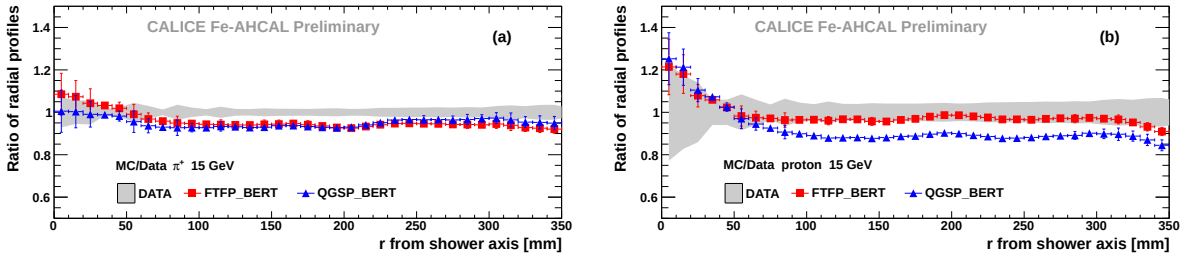

Figure 7: Ratio of radial profiles of showers induced by 15 GeV hadrons from simulated samples to those from data samples for (a) pions and (b) protons. The grey band and the error bars show uncertainty for data and simulations, respectively.

5 Parametrisation and fit of hadron shower profiles

The parametrisation is an instrument for quantitative comparison of the observed shower development with predictions of Monte Carlo models. Due to the longitudinal segmentation more than 30 points are available for the longitudinal fit up to a depth of $\sim 4.5\lambda_{\mathrm{I}}^{\mathrm{eff}}$. Each bin in longitudinal direction corresponds to $\sim 0.137\lambda_{\mathrm{I}}^{\mathrm{eff}}$. The fine transverse granularity provides more than 30 points for the radial fit in the range from 0 to 350 mm, each bin width corresponds to one third of the transverse size of the 3×3 cm^2 cell.

5.1 Fit to longitudinal profiles

The parametrisation of the longitudinal development of hadronic showers with a sum of two gamma distributions was proposed in [13] as a natural extension of the parametrisation of electromagnetic shower profiles. The application of such a parametrisation to real data usually required the convolution of this function with the exponential distribution of the shower start positions, due to impossibility to identify the shower start in the calorimeter [14]. The fine segmentation of the CALICE AHCAL gives us the unique possibility to obtain shower profiles from the shower start and parametrise them in the following way as a sum of "short" and "long" components:

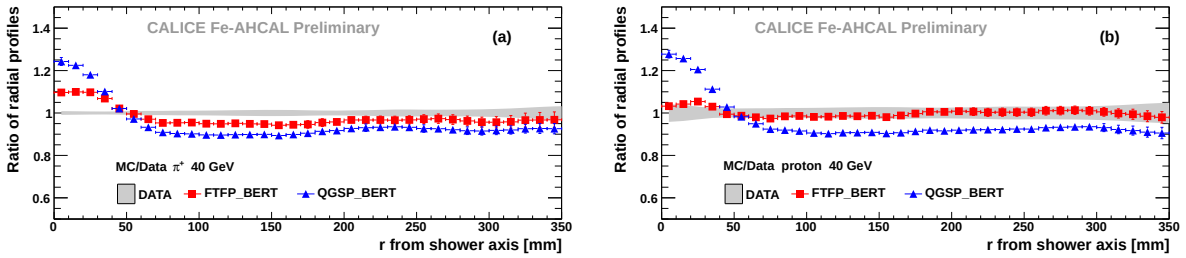

Figure 8: Ratio of radial profiles of showers induced by 40 GeV hadrons from simulated samples to those from data samples for (a) pions and (b) protons. The grey band and the error bars show uncertainty for data and simulations, respectively.

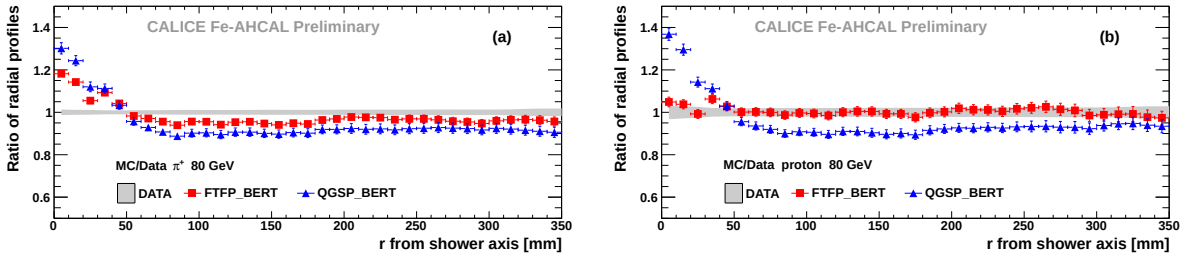

Figure 9: Ratio of radial profiles of showers induced by 80 GeV hadrons from simulated samples to those from data samples for (a) pions and (b) protons. The grey band and the error bars show uncertainty for data and simulations, respectively.

$$\Delta E(z) = A \cdot \left\{ \frac{f}{\Gamma(\alpha_{\text{short}})} \cdot \left(\frac{z}{\beta_{\text{short}}}\right)^{\alpha_{\text{short}}-1} \cdot \frac{e^{-\frac{z}{\beta_{\text{short}}}}}{\beta_{\text{short}}} + \frac{1-f}{\Gamma(\alpha_{\text{long}})} \cdot \left(\frac{z}{\beta_{\text{long}}}\right)^{\alpha_{\text{long}}-1} \cdot \frac{e^{-\frac{z}{\beta_{\text{long}}}}}{\beta_{\text{long}}} \right\}, \tag{2}$$

where A is a scaling factor, f is the fractional contribution of the "short" component with shape parameter α_{short} and slope parameter β_{short}, α_{long} and β_{long} are the shape and slope parameters of the "long" component.

The upper limit of the fit range for the longitudinal profile is determined by the chosen range of shower start positions. So only bins that belong to the AHCAL are used for the fit and the longitudinal fit range in the current analysis corresponds to the depth of $\sim 4.5\lambda_{\text{I}}^{\text{eff}}$ from the shower start. The systematic uncertainties are estimated as described above in section 3 and are summed up in quadrature to the statistical uncertainties. The smaller slope parameter from the fit is called β_{short} with the corresponding α_{short} and the fractional contribution f. Examples of fits to longitudinal profiles are shown in Fig. 10, 11 and 12, for both pions and protons.

The obtained parameters from the fit to longitudinal profiles are listed in tables 2, 3 and 4.

5.2 Fit to radial profiles

A transverse distribution of the energy density can be parametrised with a sum of a "core" component near the shower axis and a "halo" component far from the shower axis, as follows:

$$\frac{\Delta E}{\Delta S}(r) = A_{\text{core}} \cdot e^{-\frac{r}{\beta_{\text{core}}}} + A_{\text{halo}} \cdot e^{-\frac{r}{\beta_{\text{halo}}}} \tag{3}$$

where $\Delta S = 2\pi r \Delta r$ is the area of the ring of width Δr at the distance r from the shower axis, A_{core} and A_{halo} are scaling factors, β_{core} and β_{halo} are slope parameters. In the current analysis the bin width $\Delta r = 10$ mm is used. The estimated accuracy of the determination of the position of the shower axis is $\sigma_r = 2$ mm. The points on the AHCAL perimeter containing 12×12 cm^2 cells were excluded from the fit to radial profiles, limiting the radial fit range to 340 mm. The smaller slope parameter from the fit is called β_{core}. The systematic uncertainties are estimated as described above in section 3 and are summed up in quadrature to the statistical uncertainties.

Examples of fits to radial profiles are shown in Fig. 13 for both pions and protons. The scale parameters A_{core} and A_{halo} indirectly represent the energy scale. The observable which characterises the fractional contribution of the core component to the total shower energy is called "core fraction" (CF) and is estimated as follows:

$$\text{CF} = \frac{\int_0^{R_{\text{max}}} A_{\text{core}} \cdot e^{-\frac{r}{\beta_{\text{core}}}} \cdot r\, dr}{\int_0^{R_{\text{max}}} \left(A_{\text{core}} \cdot e^{-\frac{r}{\beta_{\text{core}}}} + A_{\text{halo}} \cdot e^{-\frac{r}{\beta_{\text{halo}}}} \right) \cdot r\, dr} \tag{4}$$

where R_{max} is the radial size (half width) of the AHCAL. The estimated values of the core fraction for pion showers vary from ∼60% to ∼70% (see legend in Fig. 13) in the energy range studied and are ∼5-10% lower for proton showers.

It should be noted that to obtain a stable fit procedure and reliable error estimates, no parameter limits are applied during the minimisation. Instead, a random variation of initial values for the minimisation procedure was used. From the sample of 100 attempts the best fit was chosen, the results with unphysical values were rejected. The fit quality is illustrated in Fig. 14, where the obtained values of $\frac{\chi^2}{NDF}$ are shown for all fits. A very low fraction of the "short" component in proton showers at 10 GeV does not allow to reliably separate it within given uncertainties for data and FTFP_BERT physics list, so the fit parameters for protons at 10 GeV are not compared. The very low values of $\frac{\chi^2}{NDF}$ for fits to proton data in Fig. 14a are due to large uncertainties from pion contamination which might be overestimated.

The obtained parameters from the fit to radial profiles are listed in tables 2, 3 and 4.

Table 2: Parameters from the fit to the longitudinal and radial profiles extracted from the data samples.

p_{beam}, GeV/c	α_{short}	β_{short}, X_0^{eff}	f, %	α_{long}	β_{long}, $\lambda_{\mathrm{I}}^{\mathrm{eff}}$	β_{core}, mm	β_{halo}, mm
Proton							
10	-	-	-	0.94±0.05	1.29±0.07	29.8±2.2	84.0±6.3
15	12.25±7.50	0.46±0.29	0.05±0.02	1.10±0.03	1.25±0.05	27.3±1.3	83.8±3.5
30	5.69±1.22	1.17±0.27	0.12±0.02	1.32±0.02	1.29±0.03	22.2±0.6	76.3±1.5
40	5.82±1.54	1.18±0.33	0.11±0.02	1.43±0.03	1.28±0.03	22.0±0.6	76.5±1.6
50	5.20±1.22	1.32±0.34	0.12±0.02	1.48±0.03	1.31±0.04	21.7±0.6	75.6±1.6
60	4.52±0.97	1.64±0.41	0.14±0.02	1.53±0.03	1.29±0.04	21.2±0.6	75.5±1.4
80	4.45±0.92	1.72±0.42	0.14±0.02	1.60±0.03	1.29±0.04	20.8±0.5	74.2±1.4
π^+							
10	4.55±0.54	1.44±0.18	0.19±0.02	0.92±0.02	1.30±0.04	25.0±0.7	81.4±2.0
15	4.48±0.39	1.50±0.14	0.20±0.02	1.10±0.02	1.22±0.03	23.4±0.6	77.6±1.5
30	4.45±0.29	1.63±0.12	0.23±0.01	1.35±0.01	1.24±0.02	20.6±0.5	76.0±1.2
40	4.33±0.28	1.75±0.13	0.23±0.01	1.44±0.01	1.27±0.02	20.2±0.5	74.9±1.1
50	4.19±0.25	1.87±0.13	0.24±0.01	1.50±0.01	1.27±0.02	19.9±0.4	74.3±1.0
60	4.22±0.30	1.89±0.16	0.23±0.01	1.56±0.02	1.24±0.02	19.7±0.4	74.3±1.0
80	4.36±0.31	1.89±0.16	0.23±0.01	1.61±0.01	1.26±0.02	19.5±0.4	73.9±1.0

Table 3: Parameters from the fit to the longitudinal and radial profiles extracted from the samples simulated using the FTFP_BERT physics list.

p_{beam}, GeV/c	α_{short}	β_{short}, X_0^{eff}	f, %	α_{long}	β_{long}, $\lambda_{\text{I}}^{\text{eff}}$	β_{core}, mm	β_{halo}, mm
Proton							
10	22.53±5.53	0.26±0.06	0.03±0.00	0.96±0.01	1.19±0.01	27.1±0.8	83.1±2.0
15	10.53±1.10	0.58±0.06	0.06±0.00	1.10±0.01	1.22±0.01	25.7±0.7	81.4±1.6
30	6.55±0.64	1.09±0.12	0.10±0.01	1.34±0.01	1.27±0.02	21.9±0.6	77.0±1.2
40	5.29±0.44	1.43±0.14	0.12±0.01	1.43±0.01	1.30±0.02	21.5±0.5	76.8±1.2
50	5.00±0.43	1.57±0.16	0.14±0.01	1.47±0.01	1.37±0.03	21.1±0.5	76.1±1.2
60	5.17±0.37	1.53±0.13	0.14±0.01	1.52±0.02	1.33±0.02	20.8±0.5	75.8±1.2
80	4.88±0.53	1.67±0.21	0.14±0.01	1.59±0.02	1.34±0.04	20.4±0.5	74.1±1.3
π^+							
10	6.49±0.60	1.00±0.09	0.13±0.01	0.96±0.01	1.21±0.02	23.9±0.7	77.9±1.5
15	6.17±0.43	1.09±0.08	0.17±0.01	1.12±0.01	1.19±0.02	22.6±0.6	77.3±1.3
30	4.45±0.21	1.74±0.10	0.27±0.01	1.32±0.02	1.30±0.03	19.9±0.5	75.7±1.1
40	4.80±0.21	1.63±0.08	0.26±0.01	1.44±0.02	1.25±0.02	19.2±0.5	74.4±1.1
50	4.47±0.17	1.83±0.08	0.28±0.01	1.48±0.02	1.31±0.03	19.0±0.4	74.0±1.1
60	4.57±0.20	1.78±0.09	0.28±0.01	1.53±0.02	1.29±0.03	18.8±0.4	73.6±1.1
80	4.30±0.16	1.98±0.09	0.31±0.01	1.56±0.02	1.37±0.04	18.4±0.4	73.1±1.0

Table 4: Parameters from the fit to the longitudinal and radial profiles extracted from the samples simulated using the QGSP_BERT physics list.

p_{beam}, GeV/c	α_{short}	β_{short}, X_0^{eff}	f, %	α_{long}	β_{long}, $\lambda_{\text{I}}^{\text{eff}}$	β_{core}, mm	β_{halo}, mm
Proton							
10	9.84±1.23	0.63±0.08	0.07±0.01	0.96±0.01	1.19±0.02	27.0±0.9	83.4±2.1
15	7.81±0.83	0.79±0.09	0.08±0.01	1.07±0.01	1.29±0.02	25.0±0.7	81.8±1.7
30	3.96±0.22	1.73±0.11	0.23±0.01	1.35±0.02	1.24±0.02	20.6±0.5	76.3±1.2
40	3.78±0.18	1.93±0.11	0.26±0.01	1.45±0.02	1.25±0.02	20.2±0.5	76.4±1.1
50	4.14±0.22	1.77±0.11	0.24±0.01	1.55±0.02	1.18±0.02	19.6±0.5	74.9±1.1
60	3.78±0.19	2.04±0.13	0.27±0.02	1.58±0.02	1.22±0.03	19.4±0.5	74.6±1.1
80	4.00±0.22	2.01±0.14	0.28±0.02	1.63±0.02	1.24±0.03	19.0±0.4	74.5±1.2
π^+							
10	5.42±0.55	1.16±0.11	0.15±0.01	0.92±0.01	1.20±0.02	24.9±0.8	80.1±1.9
15	4.82±0.29	1.37±0.08	0.20±0.01	1.08±0.01	1.23±0.02	22.9±0.6	78.9±1.5
30	3.89±0.14	1.88±0.07	0.36±0.01	1.33±0.02	1.30±0.03	18.9±0.5	74.4±1.1
40	3.90±0.12	1.96±0.07	0.37±0.01	1.47±0.02	1.23±0.03	18.3±0.4	74.2±1.0
50	3.86±0.14	2.06±0.09	0.39±0.01	1.48±0.02	1.32±0.04	18.4±0.4	74.7±1.1
60	4.06±0.15	1.97±0.09	0.35±0.01	1.54±0.02	1.26±0.03	17.9±0.4	73.1±1.1
80	4.12±0.18	2.00±0.11	0.35±0.02	1.60±0.02	1.26±0.04	17.7±0.4	72.7±1.0

6 Comparison of shower profile parameters

The parametrisation of shower profiles provides the possibility for quantitative comparisons of parameters which characterise the shower development. The characteristic slope values for "short" and core components are $\sim 1.5 X_0^{\rm eff}$ and $\sim 1 R_{\rm M}^{\rm eff}$ respectively, comparable with the spatial parameters of electromagnetic showers. In the tail or halo region slope parameters are 10 and 4 times larger for longitudinal and radial profiles, respectively.

6.1 Tail and halo parameters

The behaviour of the shape parameter $\alpha_{\rm long}$ shown in Fig. 15 does not depend on the particle type, is well predicted by Monte Carlo and rises logarithmically with energy. The energy dependence of "long" and "halo" slope parameters is shown in Fig. 16 and 17. These slope parameters are also well predicted by simulations. They demonstrate no energy dependence and are very similar for pions and protons. Such a behaviour supports the general idea that both the shower tail and halo consist of secondary particles which have already "forgotten" the energy and type of the initial particle.

6.2 "Short" and core parameters

The parameter $\beta_{\rm core}$ characterises the transverse shower development near the shower axis and is probably related to the angular distribution of secondary π^0s from the first inelastic interaction. The behaviour of this parameter is shown in Fig. 18. It decreases with energy, the decrease being very slow above 20 GeV. It is well predicted by both physics lists below 20 GeV and for protons by FTFP_BERT in the studied energy range. The underestimation of the slope in the core region by the FTFP_BERT physics list is $\sim$5% for pions above 20 GeV and $\sim$10% by QGSP_BERT for both particle types.

The "long" component of the longitudinal profile which dominates in the shower tail, is accompanied around shower maximum by the "short" component. The energy dependence of the "short" parameters is shown in Fig. 19 and 20. Unfortunately, the unreliable estimates for protons due to low contribution from "short" component do not allow to compare these values at low energies. Both "short" parameters for pions are well predicted by Monte Carlo except for FTFP_BERT at 10 GeV and are energy independent above 20 GeV. The position of the maximum of the "short" component $Z_{\rm max}^{\rm short}$ can be calculated as follows:

$$Z_{\rm max}^{\rm short} = (\alpha_{\rm short} - 1) \times \beta_{\rm short} \tag{5}$$

Fig. 21 shows the comparison of $Z_{\rm max}^{\rm short}$ extracted from the "short" component of pion showers with the estimation of the shower maximum position $Z_{\rm max}$ obtained from pure

electromagnetic showers induced by single electrons or positrons in the Sc-Fe AHCAL [9, 15]. In case of pions, the reconstructed energy corresponding to the integral under the "short" component is calculated using the factor 0.02364 GeV/MIP [4]. The maximums of the longitudinal profiles obtained for single electrons or positrons are shown versus the mean reconstructed energy of the corresponding particles which coincides with the beam energy within 1-2%. The position of the maximum of the "short" component for pions is calculated w.r.t. the shower start that corresponds to the estimates of $Z_{\max}$ from the calorimeter front for single electrons. The difference between $Z_{\max}^{\text{short}}$ and $Z_{\max}$ increases with decreasing energy for both data and simulations.

While the slope and shape parameters extracted from data and simulations coincide within uncertainties, the fractional contribution f of the "short" component is overestimated by both studied physics lists above 20 GeV for pions and slightly underestimated below 20 GeV. The behaviour of the parameter f is shown in Fig. 22. The FTFP_BERT physics list gives a good prediction for protons while it overestimates the parameter for pions at higher energies by 5-25%. The QGSP_BERT physics list significantly overestimates the contribution of the "short" component above 20 GeV for both pions and protons, the overestimation reaching up to 50%.

The fractional contribution of the "short" component in proton showers is approximately half of that in pion showers, as expected. Such a behaviour can be explained by a smaller electromagnetic fraction in proton showers due to lower amount of produced π^0's.

7 Conclusion

We have studied the spatial development of hadronic showers in the CALICE scintillator-steel analogue hadronic calorimeter. The fine longitudinal and radial segmentation of the CALICE AHCAL allows a comparison of shower profiles plotted from the shower start identified on an event-by-event basis. A shower parametrisation was used to perform a detailed comparison with simulated samples as well as to compare the behaviour for different types of hadrons. We analysed positive hadron data collected at beam energies from 10 to 80 GeV and simulated samples generated using the FTFP_BERT and QGSP_BERT physics lists from GEANT4 version 9.6.

The longitudinal profiles are parametrised with the sum of two contributions (gamma distributions) called "short" and "long". The parameters of the "short" component are comparable with those of electromagnetic showers, therefore this component can be considered to represent the contribution of electromagnetic showers from π^0 decays. The spatial parameters of the longitudinal tail are well reproduced by simulations. The behaviour of the tail parameters is very similar for pions and protons and does not contradict the common view that the shower tail is a complex environment of secondaries which have no memory of the primary conditions. Proton profiles are characterised by a smaller fractional contribution f of the so called "short" component. The parameter f for pions is overestimated by simulations above 20 GeV and exhibits a much steeper rise than ob-

served in data. This leads to a steeper behaviour of the predicted calorimeter response to pions.

The radial profiles are parametrised with the sum of two exponential functions which describe the behaviour near the shower axis ("core" region) and in the periphery ("halo" region). While the halo slope parameter is well reproduced by simulations, the core slope parameter is underestimated by ∼5% for pions by FTFP_BERT and by ∼10% by QGSP_BERT for both types of hadrons resulting in an underestimation of the shower width (shower radius) observed in the previous studies [12].

Our previous study presented in [3] has shown that the more recent version 9.6 of GEANT4 is closer to data than the previous version 9.4. At the same time, the behaviour observed in the current analysis for the version 9.6 is similar to that shown in [12] for the version 9.4: the overestimation of the shower core and underestimation of the shower radius for pions increase with energy. The FTFP_BERT physics list from GEANT4 version 9.6 gives very good predictions of both longitudinal and radial shower development for protons over the full studied energy range and demonstrates better agreement with data than the QGSP_BERT physics list for both pions and protons.

Acknowledgements

The author would like to thank Sergey Morozov for providing the simulated samples and is very grateful to Vasiliy Morgunov for many fruitful discussions.

References

[1] P. Adragna, *Measurement of pion and proton response and longitudinal shower profiles up to 20 nuclear interaction lengths with the ATLAS Tile calorimeter*, Nucl. Instrum. Meth. **A615** (2010) 158181.

[2] S. Agostinelli *et al.* [GEANT4 Collaboration], *Geant4: A Simulation toolkit*, Nucl. Instrum. Meth. **A506** (2003) 250.

[3] The CALICE Collaboration, *Pion and proton showers in the CALICE scintillator-steel AHCAL: comparison of global observables*, CALICE Analysis Note CAN-040 (2013).

[4] C. Adloff *et al.* [CALICE collaboration] *Hadronic energy resolution of a highly granular scintillator-steel calorimeter using software compensation techniques*, 2012 JINST **7** P09017.

[5] C. Adloff *et al.* [CALICE collaboration], *Design and electronics commissioning of the physics prototype of a Si-W electromagnetic calorimeter for the International Linear Collider*, 2008 JINST **3** P08001.

[6] C. Adloff *et al.* [CALICE collaboration], *Construction and commissioning of the CALICE analog hadron calorimeter prototype*, 2010 JINST **5** P05004.

[7] C. Adloff *et al.* [CALICE collaboration], *Construction and performance of a silicon photomultiplier/extruded scintillator tail-catcher and muon-tracker*, 2012 JINST **7** P04015.

[8] P. Mora de Freitas and H. Videau, *Detector simulation with MOKKA /GEANT4: Present and future*, LC-TOOL-2003-010.

[9] N. Feege, *Low-energetic hadron interactions in a highly granular calorimeter*, DESY-THESIS-2011-048.

[10] The CALICE Collaboration, *Local and global software compensation approaches: application to test beam data*, CALICE Analysis Note CAN-035 (2011).

[11] The CALICE Collaboration, *Pion Showers in the CALICE AHCAL Prototype*, CALICE Analysis Note CAN-026 (2011).

[12] C. Adloff *et al.* [CALICE collaboration], *Validation of GEANT4 Monte Carlo Models with a Highly Granular Scintillator-Steel Hadron Calorimeter*, 2013 JINST **8** P07005.

[13] R.K. Bock, T. Hansl-Kozanecka, T.P. Shah, Nucl. Instr. and Meth. **186** (1981) 533.

[14] P. Amaral *et al.*, *Hadronic Shower Development in Iron-Scintillator Tile Calorimetry*, CERN-EP/99 (1999).

[15] C. Adloff *et al.* [CALICE collaboration], *Electromagnetic response of a highly granular hadronic calorimeter*, 2011 JINST **6** P04003.

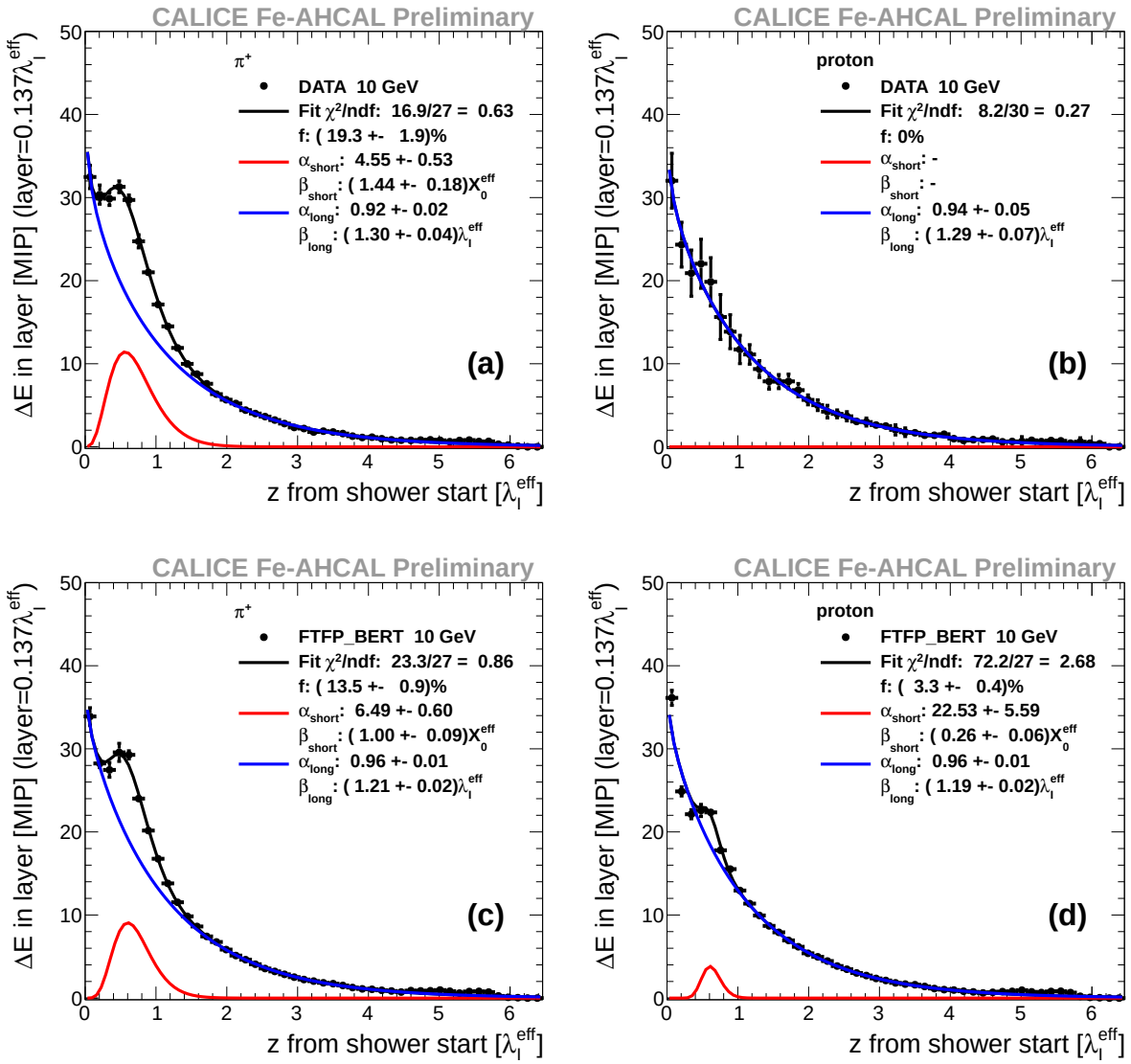

Figure 10: Fit of function (2) (black curves) to longitudinal profiles of showers initiated by (a,c) pions or (b,d) protons with initial energy 10 GeV and extracted from (a,b) data or (c,d) simulations with FTFP_BERT physics list. The red and blue curves show the contributions of the "short" and "long" components, respectively.

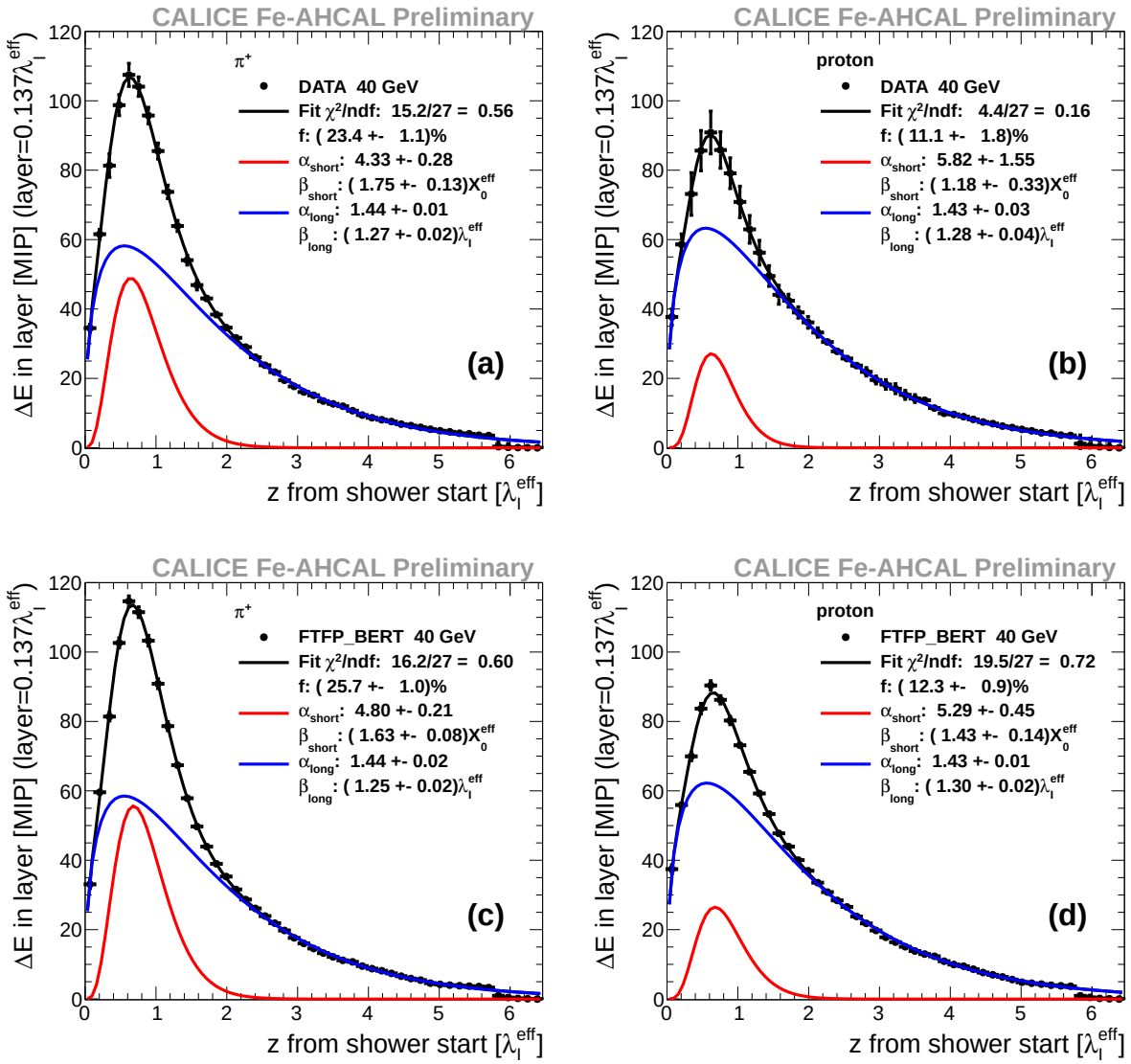

Figure 11: Fit of function (2) (black curves) to longitudinal profiles of showers initiated by (a,c) pions or (b,d) protons with initial energy 40 GeV and extracted from (a,b) data or (c,d) simulations with FTFP_BERT physics list. The red and blue curves show the contributions of the "short" and "long" components, respectively.

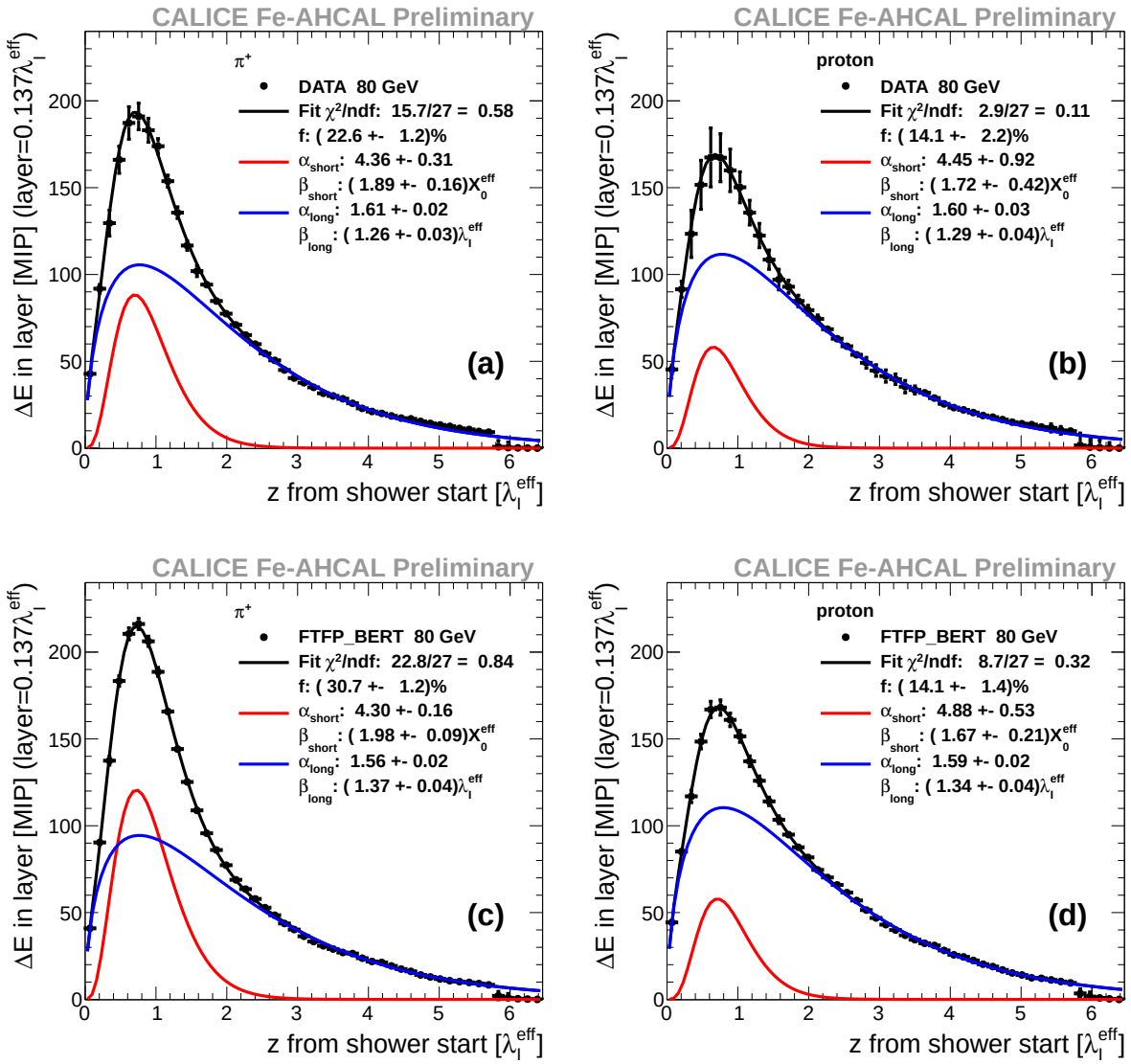

Figure 12: Fit of function (2) (black curves) to longitudinal profiles of showers initiated by (a,c) pions or (b,d) protons with initial energy 80 GeV and extracted from (a,b) data or (c,d) simulations with FTFP_BERT physics list. The red and blue curves show the contributions of the "short" and "long" components, respectively.

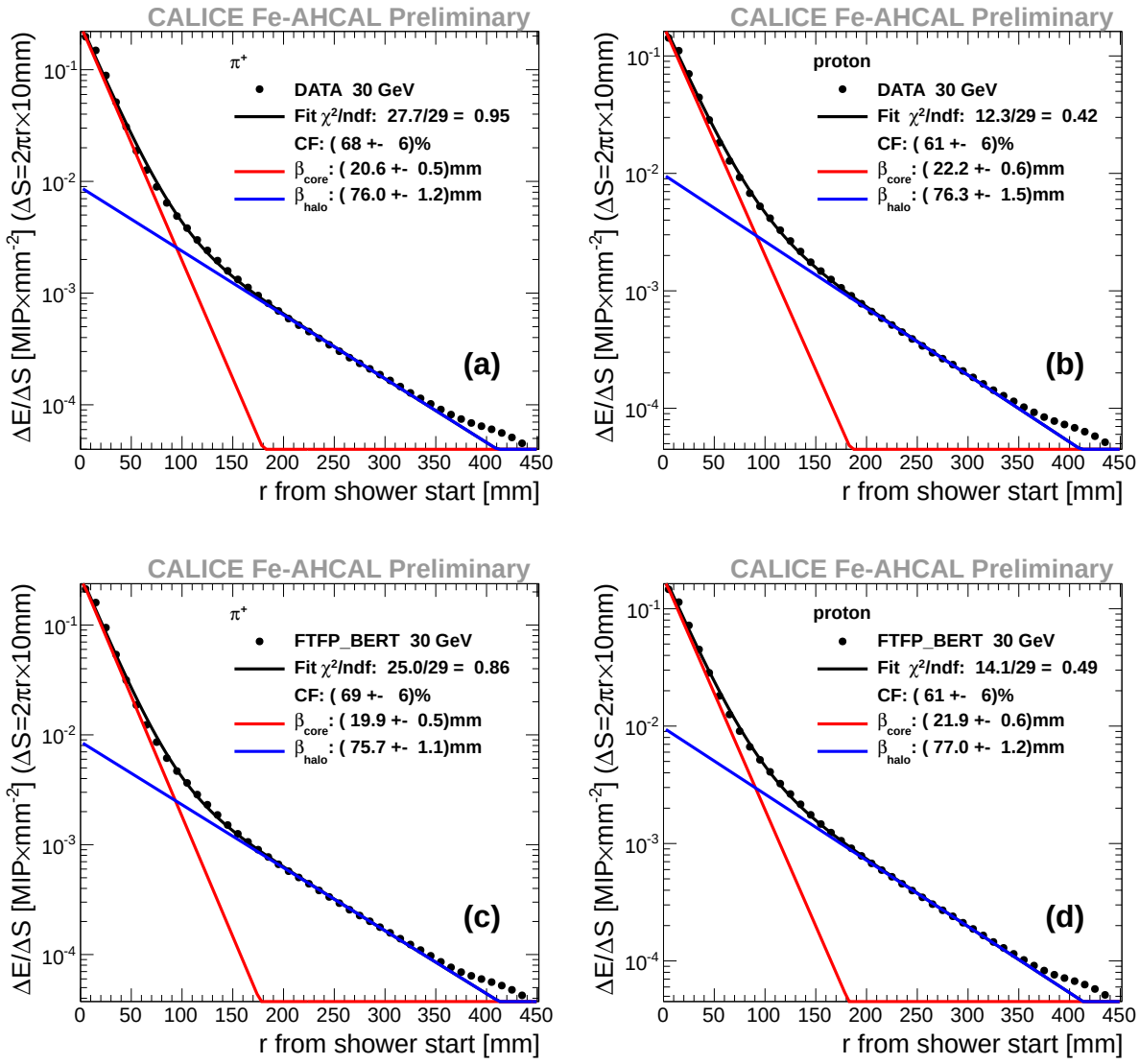

Figure 13: Fit of function (3) (black curves) to radial profiles of showers initiated by (a,c) pions or (b,d) protons with initial energy 30 GeV and extracted from (a,b) data or (c,d) simulations with FTFP_BERT physics list. The red and blue curves show the contributions of "core" and "halo" components, respectively. See text for details.

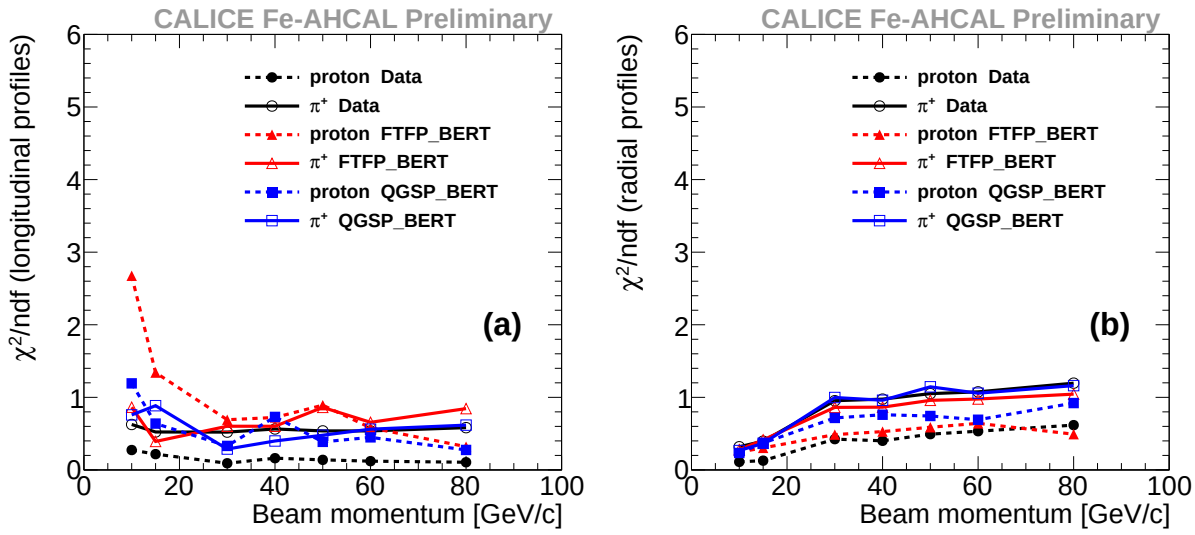

Figure 14: Energy dependence of fit quality for fit to (a) longitudinal and (b) radial profiles for data and simulations.

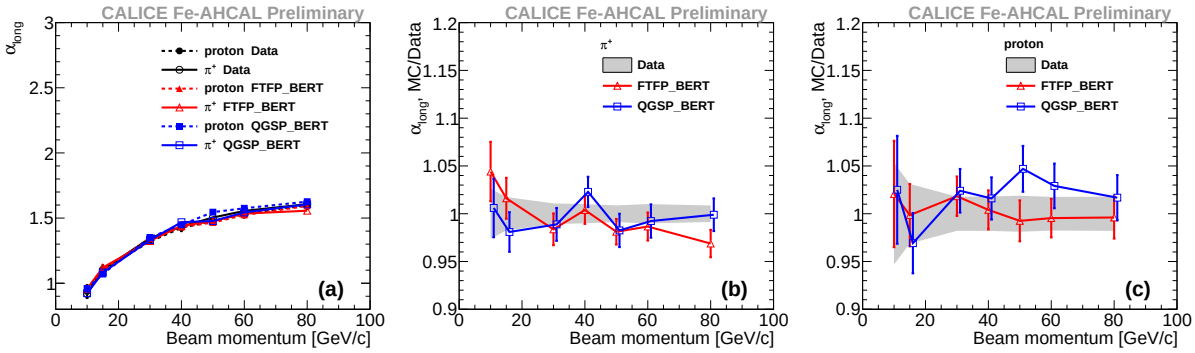

Figure 15: (a) Energy dependence of the shape parameter α_{long} and the ratio of α_{long} extracted from simulation to those extracted from data for (b) pions and (c) protons.

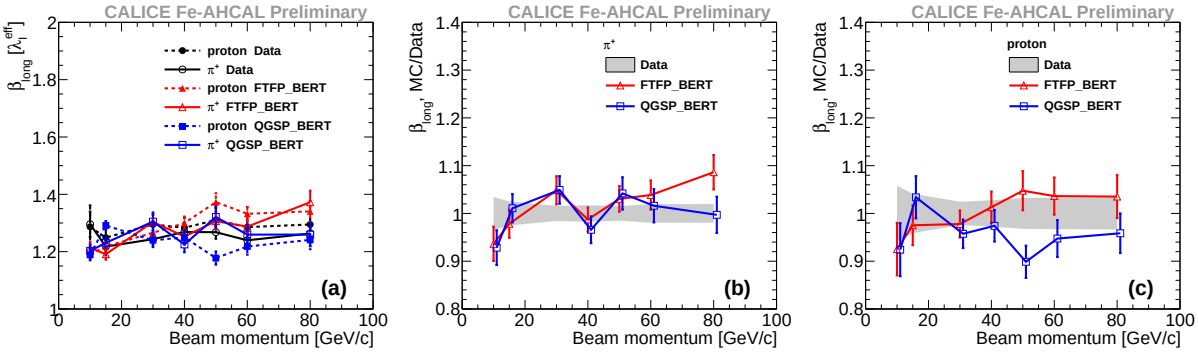

Figure 16: (a) Energy dependence of the tail slope parameter β_{long} and the ratio of β_{long} extracted from simulation to those extracted from data for (b) pions and (c) protons.

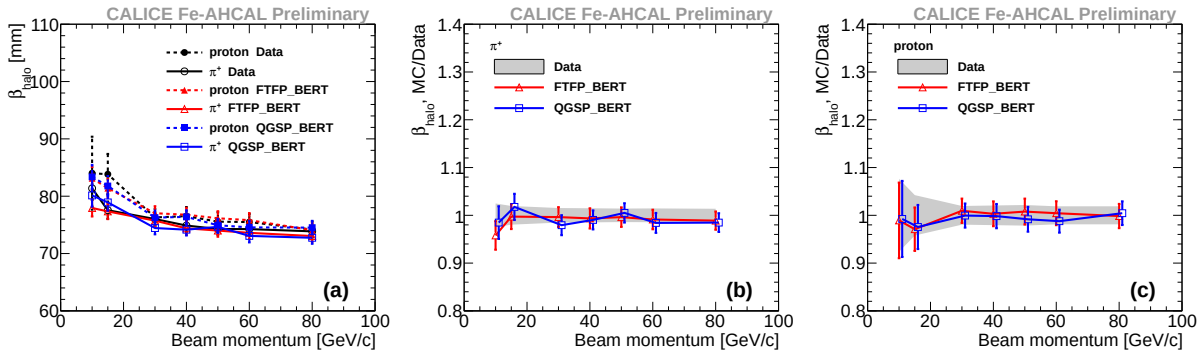

Figure 17: (a) Energy dependence of the halo slope parameter β_{halo} and the ratio of β_{halo} extracted from simulation to those extracted from data for (b) pions and (c) protons.

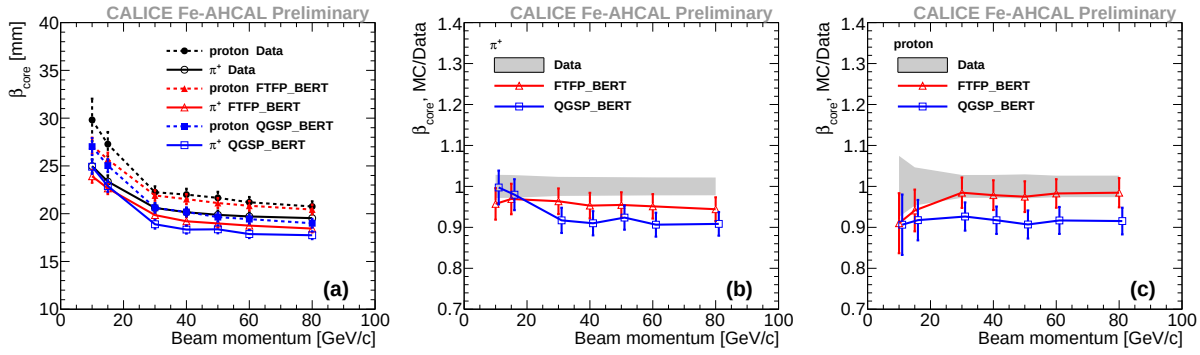

Figure 18: (a) Energy dependence of the slope parameter β_{core} and the ratio of β_{core} extracted from simulation to those extracted from data for (b) pions and (c) protons.

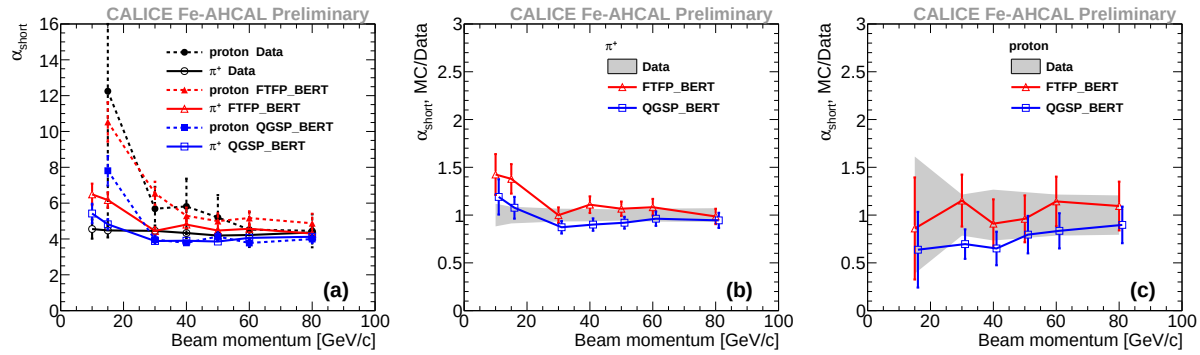

Figure 19: (a) Energy dependence of the shape parameters α_{short} and the ratio of α_{short} extracted from simulation to those extracted from data for (b) pions and (c) protons.

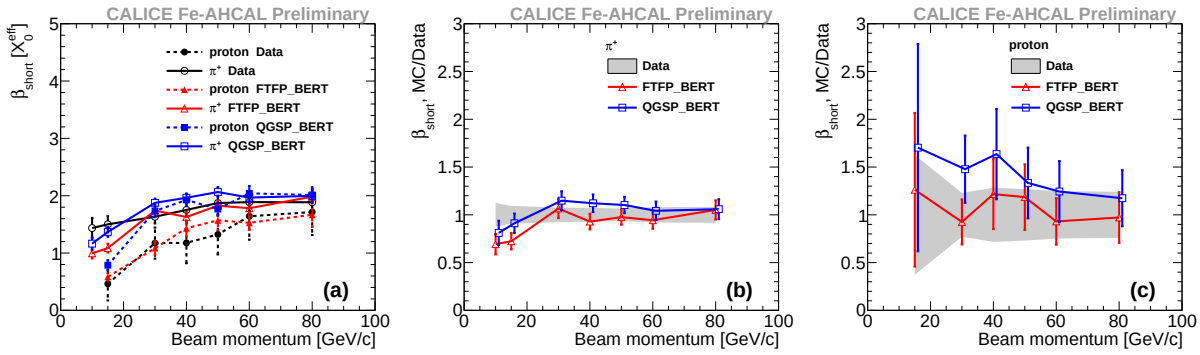

Figure 20: (a) Energy dependence of the slope parameter β_{short} and the ratio of β_{short} extracted from simulation to those extracted from data for (b) pions and (c) protons.

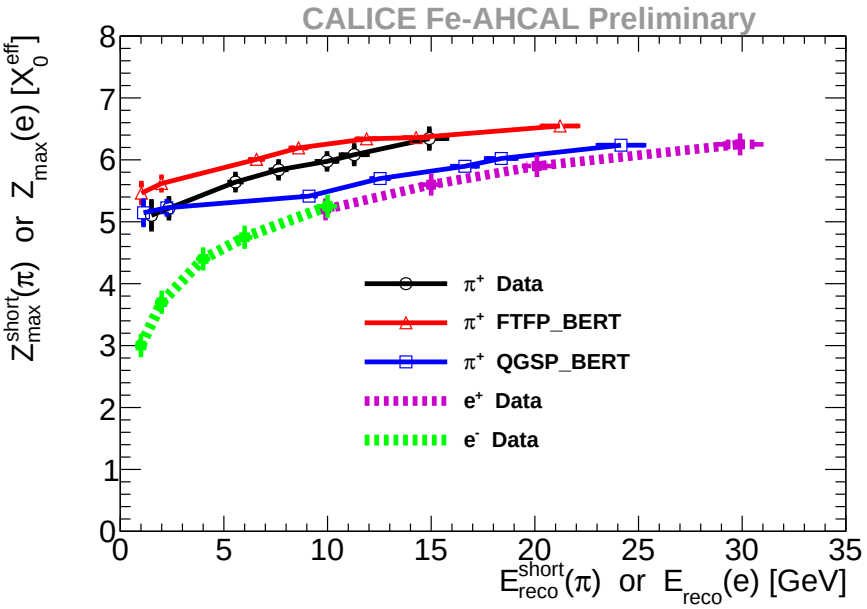

Figure 21: Solid lines: maximum of the "short" component versus energy of the "short" component estimated from the fit to pion shower profiles from data (black) and simulations with FTFP_BERT (red) and QGSP_BERT physics list (blue). Dashed lines: maximum of the longitudinal profile obtained for electromagnetic showers induced by single electrons (green) [9] or positrons (magenta) [15] in the AHCAL versus the mean reconstructed energy.

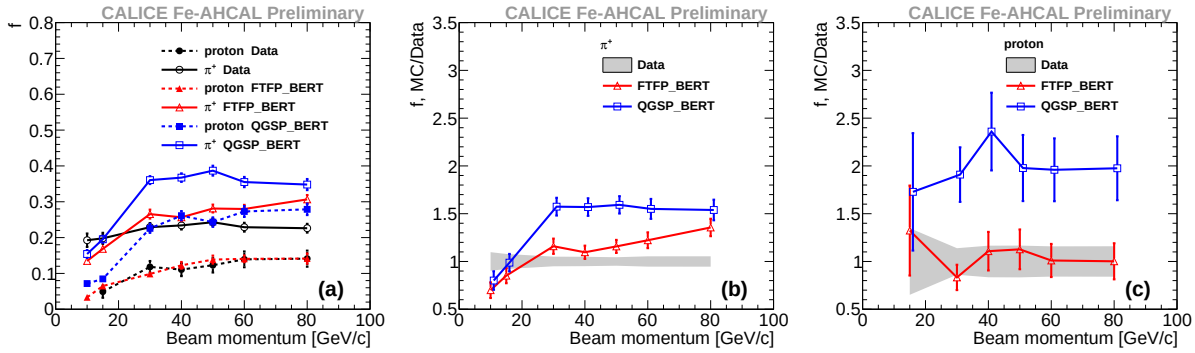

Figure 22: (a) Energy dependence of the "short" component fraction f and the ratio of f extracted from simulation to those extracted from data for (b) pions and (c) protons.